EFDA–JET–PR(09)55

A. Czarnecka, K-D Zastrow, J. Rzadkiewicz, I.H. Coffey, K.D. Lawson,
M.G. O'Mullane and JET EFDA contributors

Determination of Metal Impurity Density, ΔZ_{eff} and Dilution on JET by VUV Emission Spectroscopy

Determination of Metal Impurity Density, ΔZ_{eff} and Dilution on JET by VUV Emission Spectroscopy

A. Czarnecka[1], K-D Zastrow[2], J. Rzadkiewicz[1], I.H. Coffey[3], K.D. Lawson[2], M.G. O'Mullane[4] and JET EFDA contributors*

JET-EFDA, Culham Science Centre, OX14 3DB, Abingdon, UK

[1]Institute of Plasma Physics and Laser Microfusion, EURATOM Association, Hery 23 St, 01-497 Warsaw, Poland
[2]EURATOM-CCFE Fusion Association, Culham Science Centre, OX14 3DB, Abingdon, OXON, UK
[3]Astrophysics Research Centre, School of Mathematics and Physics, Queen's University, Belfast, BT7 1NN, Northern Ireland, UK
[4]Department of Physics, University of Strathclyde, Glasgow G4 0NG, UK
** See annex of F. Romanelli et al, "Overview of JET Results", (Proc. 22 [nd] IAEA Fusion Energy Conference, Geneva, Switzerland (2008)).*

Preprint of Paper to be submitted for publication in
Plasma Physics and Controlled Fusion

ABSTRACT.
The provision of measurements of metallic impurity densities, Z_{eff}, and dilution for a large number of discharges within a campaign facilitates the analysis of impurity trends. Such trends are of increasing importance as additional heating power and pulse length increase. This is particularly important for RF heating and therefore it is especially relevant to the assessment of the ITER-Like Antenna (ILA) on JET. To this end, a method is presented for determining the metal impurity density, ΔZ_{eff}, and dilution in steady-state JET plasmas using passive VUV emission. The method is based on the combination of absolutely calibrated VUV transition intensity measurements with Universal Transport Code (UTC) simulations. In the analysis the line integrated measurements of transitions in Li-like Ni, Fe, and Cu have been used for test discharges characterised by widely varied plasma profiles. The simulations use a wide class of transport coefficients for diffusion D(r) and convection v(r). For a given pair of D(r) and v(r), the simulated line intensity has been matched to the line intensity measured in the experiment. An approximately linear dependence of the derived metal densities, ΔZ_{eff} and dilution normalised to a Li-like line intensity on electron temperature has been obtained which is valid in a localized, mid radius plasma region. These linear dependences are exploited to derive local metal densities for JET discharges.

1. INTRODUCTION

Studies of the impurity behaviour in tokamak plasmas during additional heating are of fundamental interest because of the increased radiated power and ion dilution. In particular, mid- and high-Z impurities can contribute significantly to the average Z_{eff} during high power Radio Frequency (RF) pulses. Furthermore, VUV radiation emitted by metallic impurities at the plasma edge affects the plasma density limit and the quality of the RF-induced H-modes, and impurity release from the screens of the RF antennae may significantly limit the heating effectiveness [1].

Since metallic impurity radiation increases with RF power and pulse duration, it is especially relevant to the assessment of the ITER-Like Antenna (ILA) [2] in JET, for which powers of up to 7.2 MW are expected. Such assessment is facilitated by the provision of metallic impurity densities for large numbers of discharges and, to this end, a method for determining the densities, ΔZ_{eff}, and dilution in steady-state plasmas using passive spectroscopy is presented. In the first instance, this method has been applied to Ni [3], the most common metallic impurity observed in JET. In this article the method is also extended to other mid-Z impurities, namely Fe and Cu. Examples are shown of the application of the technique for different types of additional heating.

2. EXPERIMENTAL ARRANGEMENT

The method relies on measurements of the intensity of the radiation emitted by the metallic impurities [3]. Spectral lines from a wide range of elements and ionization stages fall in the VUV spectrum, making it a particularly valuable spectral region for diagnosing high temperature plasmas. Measurements were performed by means of a Princeton Instruments SPRED [4] spectrometer,

known in JET as KT2 [5-6]. The spectrometer typically registers VUV spectra in the wavelength range of 100–1100Å with a spectral resolution of ~5Å. The detector consists of a microchannel plate coated with CuI and a phosphor coupled by a fibre optic bundle to a 2048 photodiode array. The instrument is situated outside the torus hall, at a distance of 22 m from the plasma [5] – its installation on JET is shown in Figure 1a. The line of sight (l-o-s), shown in Figure 1b as a horizontal red line, is along the vessel midplane via a spherical mirror (Au coating) with an angle of incidence of 75^{o} that reduces the sensitivity by about 50%. The survey spectrometer is routinely used to give impurity data for the operation of the JET machine. A line integration technique was used, in which Simpson's rule is applied to the area defined by a certain number of pixels on either side of the line centre, these pixels also defining the background to be subtracted. With 2048 pixels, an integration range covering ±5 pixels from the line centre was regarded as the best compromise between minimizing blending and using a sufficient proportion of the line profile to ensure reliable measurements.

In order to fully exploit the line intensity measurements, an absolute sensitivity calibration for this spectral region has been made [5]. The relative calibration at short wavelengths has been derived by comparing measured and modelled Na- and Li-like metal line intensity ratios. The CII to CIV line intensity ratios have been used at longer wavelengths. The absolute calibration has been obtained by an *in situ* cross calibration via branching ratios to an absolutely calibrated visible spectrometer.

In the wavelength range scanned by the KT2 diagnostic one can observe six intense lines originating from the Ni impurity, four being the Li-like and Na-like doublets ($1s^2 2s\ ^2S_{1/2} - 1s^2 2p\ ^2P_{1/2,3/2}$ and $2p^6 3s\ ^2S_{1/2} - 2p^6 3p\ ^2P_{1/2,3/2}$), and another one a Mg-like line ($2p^6 3s^2\ ^1S_0 - 3s3p\ ^1P_1$). At low wavelengths the line that corresponds to the $1s^2 2s^2\ ^1S_0 - 1s^2 2s2p\ ^1P_1$ transition in Be-like Ni can also be seen, although in this range the sensitivity of the SPRED spectrometer falls off sharply, which leads to a less certain calibration. The calibration for the Li-like and Na-like doublets is most accurate, this being crucial for determining the absolute level of an impurity. In the case of Fe and Cu the corresponding transitions to those in Ni are observed. These lines can dominate the short wavelength VUV spectrum as can be seen in Figure 2, which shows intense Ni, Fe, and Cu lines recorded between 23 s and 24 s in Pulse No: 61173.

3. ANALYSIS METHOD

3.1. SPECTROSCOPIC ANALYSIS

The choice of a specific atomic transition and ion species to represent the elemental contribution to the total radiation is an important aspect of the analysis. Because the temperature in a fusion device increases from the edge to the core, the higher ionization stages dominate in the plasma centre. In JET plasmas, low-Z elements such as C are fully ionized over most of the plasma volume, while the partially ionized charge states are concentrated at the plasma edge. Medium-Z elements exist in the H-, He-, and Li-like ionization states in the core. To give an approximate idea of the relevance of the different Ni charge states to the spectroscopic analysis, which will employ a more complex model, Figure 3a shows the steady-state radial distributions of nickel, as a function of normalized

minor radius r/a, in coronal equilibrium with an electron temperature on axis $T_e(0)$ of 4keV. The edge ion (Ni^{q+}, $q \leq 24$) line intensities are prone to variation due to changes in the edge pressure profiles, influxes and recycling, and therefore they are not suitable candidates for our analysis. In the core, where the coronal model is more realistic, nickel predominantly appears in the He-like ionization stage. Unfortunately, such Ni radiation from the bulk plasma lies in the high energy x-ray region and is not monitored by the KT2 diagnostic. Nevertheless, the VUV radiation emitted from the Li-like nickel is also significant in the core, and can be used in the analysis. Since the aim of the analysis is to determine the metal impurity density in the core plasma by VUV emission spectroscopy, ion species existing in the intermediate region, approximately between $0.4 \leq r/a \leq 0.8$, are favored. The most intense lines in the VUV range, representing Li-like transitions of different metallic elements, which are listed in Table 1, have been used in the analysis. Figure 3b shows the abundance prediction in coronal equilibrium of Li-like Ni, Fe, and Cu fractions vs. electron temperature. Although this approach is not fully adequate for the mid radius region, we can deduce that for the same plasma profiles emission from the foregoing metals appears nearly in the same region. Therefore, we will use the same profiles of transport parameters for all the analyzed elements, as explained below.

Once the Li-like line intensities are matched with the transport parameters, it is possible to use them for further impurity studies. However, the ionization equilibrium balance assumption is only appropriate to ions at the centre of the discharge. Away from the plasma core transport must be considered [7], a factor that seriously complicates the routine evaluation of impurity data. Transport of particles disturbs the temperature at which the ions are situated changing the radial position of the emitting impurity.

3.2. DETERMINATION OF METAL IMPURITY DENSITY

The method used for determining the metal impurity density is based on the combination of absolutely calibrated VUV transition intensity measurements with Universal Transport Code (UTC) simulations [8]. The characteristics of the transport change across the plasma, and impurity transport can be described for different regions [9]. In the Scrape-Off-Layer (SOL) region (outside the separatrix) the transport properties are dominated by fast longitudinal transport due to open field lines and by atomic physics. In the Edge Transport Barrier (ETB) region where $0.95 \leq r/a \leq 1$ (inside the separatrix) reduced transport closer to neoclassical levels [10] has been observed. In the narrow region just inside the ETB at $0.8 \leq r/a \leq 0.95$ transport can be dominated by ELMs, collisional turbulence and charge-exchange with cold neutrals. The region $0.4 \leq r/a \leq 0.8$, which is inside our scope of interest, is characterized by anomalous transport, originating from turbulence. Finally, transport in the plasma core ($r/a \leq 0.4$) is either dominated by sawtooth instabilities in the conventional scenario or by a region with reduced anomalous transport in discharges with an Internal Transport Barrier (ITB). Impurity transport can be described by equation

$$\frac{\partial}{\partial t} n_Z^{q+} = -\frac{1}{r}\frac{\partial}{\partial r}(r\Gamma_z) + \text{Sources} - \text{Sinks} \qquad (1)$$

where n_Z^{q+} is the impurity density for a given ion charge state (q+). Sources and sinks, which are functions of electron temperature and density, include electron-impact ionisation from lower charge states and electron recombination from higher charge states.

The impurity particle flux Γ_Z can be described as a sum of diffusive and convective terms,

$$\Gamma_z = -D\frac{\partial}{\partial r}n_Z^{q+} + Vn_Z^{q+} \tag{2}$$

where D(r) is the impurity diffusion coefficient and V(r) the impurity convection velocity. A negative value of V indicates an inward particle pinch.

To run the UTC code input parameters must be provided. These include information about the plasma, namely plasma geometry, the position of the flux surfaces reconstructed with the equilibrium code EFIT, and plasma profiles (T_e, n_e) given by specific diagnostics. In order to reproduce the measured VUV line intensities, information on various atomic data and diagnostic geometry have to be taken into account. Other necessary inputs are particle influx and transport (D and V) profiles. The solution of equation (1) for given D and V gives a set of simulated impurity density profiles. These allow the calculation of individual line emission intensities and their matching to experiment. Our method is based on the hypothesis that the measured intensity I of a particular line corresponding to emission from the charge state Q+ of the element with atomic number Z can be expressed in the simple form

$$I = n_Z^{Q+} n_e F(T_e) \tag{3}$$

where is the electron density and the unspecified function of temperature $F(T_e)$ encapsulates all relevant atomic processes leading to the line emission of radiation. By further assuming that the fractional abundance of charge state $Q+$ is constant for a given temperature, the total impurity density $n_z^{Total} = \sum_{q=0}^{Z} n^{q+}$ can be written as

$$n_z^{Total} \sim n_z^{Q+} \tag{4}$$

whereby from (3) one can write that, for a fixed temperature,

$$n_Z^{Total} \sim I/n_e \tag{5}$$

The idea behind the method is to search for a simple dependence on temperature to be inferred from the experimental data on the right-hand side of (5), and from the simulation data on the left-hand side of (5). More specifically, making use of n_z^{Total} from UTC simulations, a relation between the ratio of the left-hand and right-hand sides of relation (5) and electron temperature is to be sought, which would allow the determination of the total impurity density from the experimentally measured

line intensity, electron density, and temperature. The application of this simple model to experimental data will show if the above assumptions prove to be reasonable. If that will indeed be the case, a simple formula for the total impurity density can be established with this method, as well as the limits of its application – for instance the range of radius for which the formula will be valid.
Since additional heating can be applied only in the divertor phase, the intensity of lines during that phase has been used in the simulations. L- and H-mode JET discharges characterised by widely different electron temperature and density profiles (see figure 4) have been tested. The electron temperature and density profiles were provided by the LIDAR Thomson scattering [11] and electron cyclotron emission diagnostics [12], while the atomic data for line emission coefficients, ionisation and recombination sources and sinks have been taken from the ADAS database [13].

Unlike other UTC inputs, the transport coefficients were treated as unknown parameters. In the simulations, a wide class of transport coefficients (D, V), presented in Figure 5, has been considered to assess the effect of different transport scenarios on the resulting impurity density profiles. Therefore, given the anomalous character of mid-radius transport, the transport coefficients in this region have been varied over an order of magnitude compared to neoclassical values [14, 15]. The transport coefficients were parameterised by a set of points at given discrete spatial positions r/a. These points were interpolated in order to generate the full transport coefficients. The choice of the D and V profile sets has also been inspired by previous extensive studies of metal impurity transport [16-19]. A study of the Z dependence of impurity transport shows no clear difference between L- and H-mode in the transport coefficients in the core and at mid-radius and only a weak dependence of the impurity peaking V/D with Z has been observed in the region between 0.5 and 0.6 [17]. Therefore, for all impurities the same sets of transport coefficients have been employed since we expect the emission of the lines of interest (Li-like) to be in the mid-radius region.

Since only steady-state plasmas were investigated, the diffusion and convection velocity have been kept constant in time. For a given set of D(r) and V(r), the simulated line intensity was matched to that measured in the experiment.

3.3. DETERMINATION OF ΔZ_{eff} AND DILUTION FOR METAL IMPURITIES

A parameter of great interest in the study of the behavior of impurities is the effective charge of the plasma, Z_{eff}. Several methods and plasma diagnostics exist, both passive and active, for the determination of Z_{eff}, such as line-integrated visible bremstrahlung measurements [20], and summation of impurity densities measured by Charge Exchange Spectroscopy [21]. Other diagnostics for Z_{eff} are based on measurements of plasma resistivity, continuum soft-X-rays and neutron yields. On JET, carbon is by far the dominant impurity contributing to Z_{eff}, but other impurities such as Ni, Fe, Cr, and Cu can also give an appreciable contribution to this parameter.

Z_{eff} is a local measure of the impurity concentration in the plasma, averaged over all impurities. For a plasma with a single impurity of atomic number Z_{eff} is defined by

$$Z_{eff} = 1 + \sum_{q=2}^{Z} q(q-1)\frac{n_z^{q+}}{n_e} \equiv 1 + \Delta Z_{eff} \tag{6}$$

In the right-hand side of eq. (6) the impurity concentration is dependent on line intensity according to $n_Z^{Total}/n_e \sim I/n_e^2$. Therefore, a simple dependence of the ratio of ΔZ_{eff} and I/n_e^2 on T_e, similar to the one established above for impurity concentration and discussed above apropos relation (5), can also be expected for ΔZ_{eff}.

The impurity ions in the plasma have two detrimental effects. They firstly cause additional energy losses from the plasma through radiation (i.e. bremsstrahlung, recombination and line radiation). Secondly, their electrons contribute to the plasma pressure and electron density. For a given plasma pressure or electron density the presence of impurity ions causes a dilution of the fuel species, deuterium and tritium, which reduces the fusion rate. In order to avoid these phenomena and for the realization of a burning fusion plasma it is necessary to keep the impurity concentrations below a certain critical level. Plasma dilution due to impurity ions can be expressed (in the case of a single impurity of atomic number Z) as

$$\Delta n_{HDT} = \sum_{q=0}^{Z} q \times n_z^{q+} \tag{7}$$

where by the same reasoning applied to equation (6) a simple dependence of the ratio of Δn_{HDT} and on T_e can be expected.

4. RESULTS

Examples of the total Ni density profiles obtained by means of the UTC simulations are presented in Figures 6a and 6b for the wide class of transport coefficients presented in Figures 5a and 5b, respectively. All Ni density profiles result from matching the simulated and experimental Li-like line intensity. For a wide range of sets of transport coefficients – see Figures 5a and 5b, the impurity density varies only by 10–20% at the mid-radius region, with larger variations elsewhere. In simulations with different sets of transport coefficients, it has been observed that the statistical variation at mid-radius is due to low values of D(r), and it does not increase for sets with diffusion coefficients larger than 5.

For an ion X^{q+} within a plasma at a local electron temperature and density we can calculate how many photons that ion will emit for a given transition. If we know such a quantity, called the photon emissivity coefficient (pec) and also the electron temperature, electron density, and impurity density profiles, the emissivity along the KT2 l-o-s can then be obtained:

$$\varepsilon\left(r/a\right) = \mathrm{pec}(T_e, n_e) n_Z^{q+} n_e \tag{8}$$

For each and every simulation, a parameter $\langle r/a \rangle$ weighted by the Li-like emissivity ε, has been

calculated and used to assign the simulated impurity density, as well as the electron temperature and density,

$$\left\langle r/a \right\rangle = \frac{\int_{\Gamma} r/a \, \varepsilon dl}{\int_{\Gamma} \varepsilon dl} \tag{9}$$

where Γ is the KT2 l-o-s, to which r/a values are mapped, and ε is the emissivity of the Li-like ion stage.

It has been found that in all simulations and for all the analysed pulses the $\langle r/a \rangle \sim 0.5$-$0.6$. In this region local electron temperatures range from 2 to 4.7 keV (see Figure 4a).

Figure 7 shows the average ratio of the simulated impurity density to the experimental line intensity for Li-like Ni, Fe, and Cu normalized to the electron density for the $\langle r/a \rangle$ as a function of the electron temperature. Each point in this figure corresponds to one plasma discharge characterised by different plasma parameters. Error bars reflect the variation of transport coefficients and electron temperature, the latter occurring when averaging over the different simulations of the plasma discharge at the simulation-dependent $\langle r/a \rangle$ of emissivity. An approximately linear dependence on the local electron temperature of the ratio between the derived Ni, Fe, and Cu densities and the suitable line intensity has been obtained for r/a ~ 0.5 - 0.6. A difference has been observed in the linear fitting between points corresponding to L- and H-mode. However, this difference is within the range of the error bars and can be neglected. Moreover, an analysis has been conducted with transport coefficients that vary their shape widely along the normalized radius r/a. This study showed that all reasonable transport coefficients resulted in a good matching to the linear trend.

Also an approximately linear dependence on the local electron temperature of the ratio between the derived metal ΔZ_{eff}, dilution and the line intensity has been obtained for the same radius. Results are shown in figure 8 and 9, respectively.

The linear fits for a selected impurity in Figure 7 are exploited to derive local metal impurity density for all JET discharges during the divertor phase. The linear fits in Figure 8 are exploited to derive ΔZ_{eff} and the linear fits from figure 9 to derive dilution. The coefficients of the linear fits in temperature of the derived quantities: density, ΔZ_{eff} and dilution, and their respective errors are listed in Table 2 for Ni, Fe, and Cu.

For every quantity a Z-dependence behaviour has been observed. Through the fit coefficients the equation for total impurity density (10), ΔZ_{eff} (11) and dilution (12) as a function of Z can be written in the form

$$n_Z^{Total}(Z) = \left[(a_1 + a_2 * Z) + (b_1 + b_2 * Z) * T_e\right] * \frac{I}{n_e} \tag{10}$$

where $a_1 = -7.3 \cdot 10^{16}$, $a_2 = 3.3 \cdot 10^{15}$, $b_1 = 1.2 \cdot 10^{17}$, $b_2 = -3.3 \cdot 10^{15}$, Z is the atomic number, I is the calibrated line intensity, T_e is the electron temperature, and n_e is electron density;

$$\Delta Z_{eff}(Z) = \left[(c_1 + c_2 * Z) + (d_1 + d_2 * Z) * T_e\right] * \frac{I}{n_e^2} \tag{11}$$

where $c_1 = -4.4 \cdot 10^{19}$, $c_2 = 1.7 \cdot 10^{18}$, $d_1 = 1.9 \cdot 10^{19}$ and, $d_2 = 1.9 \cdot 10^{19}$ and

$$\Delta n_{HDT}(Z) = [(i_1 + i_2 * Z) + (j_1 + j_2 * Z) * T_e] * \frac{I}{n_e} \quad (12)$$

where $i_1 = -3.6 \cdot 10^{18}$, $i_2 = 1.4 \cdot 10^{17}$, $j_1 = 2.5 \cdot 10^{18}$ and, $j_2 = -5.6 \cdot 10^{16}$.

Using the above equations it is possible to apply the method to additional elements given their atomic number Z. Linear fits for the impurity density, ΔZ_{eff}, and dilution have been obtained for Cr, a medium Z impurity that is commonly observed in JET plasmas, and presented in Figures 7–9 (green line). The direct impurity analyses for Cr were not possible because of the lack of the proper atomic data.

5. APPLICATION OF THE METHOD

The method has been used to study the behaviour of the Ni impurity density with applied heating power in JET. The different heating systems, namely the A2 Ion Cyclotron Resonance Heating (ICRH) antennae, the new ITER-like ICRH antenna (ILA) (up to 4.76MW coupled in L-mode), the Lower Hybrid Current Drive (LHCD), and the Neutral Beam Injection (NBI) system have been considered separately. This has been achieved by carefully choosing time ranges in selected JET pulses for which only one heating system was in use. Moreover, during these time ranges the plasma remained in steady-state, and average values of I, n_e, T_e and heating power have been retrieved for the analysis. Concerning the ICRH systems, each of the four A2 antennae has a surface of 2.25m^2, much larger than the 0.91m^2 of the ILA. The A2 system can operate with a power density up to 1.8MW/m^2 [22, 23]. A database has been built with data from selected L-mode plasmas from the restart of 2005 to October 2009 (JET Pulse No's: 66080–78157) in the case of the A2 antennae, and from May 2008 to October 2009 (JET Pulse No's: 73000–78157) in the case of the ILA see Figure 10. It can be seen that for the same total power–but at a much higher power density up to 6.2 MW/m^2 the ILA performs well, with a low release of impurities into the core plasma in comparison with the A2 antennae. Moreover, Figure 10 also shows that for the same power the impurity release with ICRH is much higher than with LHCD (JET Pulse No's: 65696–77744) or NBI heating (JET Pulse No's: 65694–78148).

CONCLUSIONS

The aim of this paper is to establish a method to allow the determination of the metal impurity density in JET plasmas from spectroscopy measurements. The VUV line intensity for Li-like transitions in Ni, Fe, and Cu has been reproduced with UTC for a wide class of transport coefficients. From the dependence of the ratio between the derived impurity densities and the line intensity on local electron temperature, a linear fit has been established allowing the calculation of the local impurity density in the region with normalized radius from 0.5 to 0.6. Based on the same method,

linear fits in temperature have been established for other quantities, namely ΔZ_{eff} and dilution. These linear dependences have been exploited to derive local metal densities, ΔZ_{eff}, and dilution for large sets of JET discharges. In particular, the method has been applied to study the behaviour of impurities with ICRH power from the A2 and ILA antennae, which demonstrates the lower metallic impurity release of the ILA antennae.

ACKNOWLEDGMENTS

This work, supported by the European Communities under the contract of Association between EURATOM and IPPLM, was carried out within the framework of the European Fusion Development Agreement. The views and opinions expressed herein do not necessarily reflect those of the European Commission.

REFERENCES

[1]. Bures M. *et al* 1991 *Plasma Physics and Controlled Fusion* **33** 937
[2]. Durodie F. *et al* 2005 *Fusion Engineering and Design* **74** 223
[3]. Czarnecka A. *et al* 2009 *36th EPS Conference* ECA vol. **33E** P-2.146
[4]. Fonck R.J. *et al* 1982 *Applied Opt*ics **21** 2115
[5]. Lawson K.D. *et al* 2009 JINST **4** P04013
[6]. Coffey I.H. *et al* 2004 *Review of Scientific Instruments* **75** 3737
[7]. Stratton B.C. *et al* 2008 *Fusion Science and Technology* **53** 431
[8]. Whiteford A.D. *et al* 2004 *31st EPS Conference* ECA vol. **28G** P–1.159
[9]. Parail V.V. 2002 *Plasma Phys. Control. Fusion* **44** A63
[10]. Hirshman S.P. and Sigmar D.J. 1981 *Nucl. Fusion* **21** 1079
[11]. Gowers C. *et al* 1995 *Rev. Sci. Instrum.* **66** 471
[12]. De La Luna E *et al* 2004 *Rev. Sci. Instrum.* **75** 3831
[13]. Summers H.P. 2000 *The ADAS User Manual version 2.7* http://www.adas.ac.uk
[14]. Pasini D. *et al* 1990 *Nuclear Fusion* **30** 2049
[15]. Giannella R. *et al* 1994 *Nuclear Fusion* **34** 1185
[16]. Giroud C. *et al* 2004 *31st EPS Conference* ECA vol. **28G** P–5.159
[17]. Giroud C. *et al* 2007 *34th EPS Conference* ECA vol. **31F** P-2.049
[18]. Carraro L. *et al* 2007 *34th EPS Conference* ECA vol. **31F** O-4.028
[19]. Guirlet R. *et al* 2000 *Fusion Energy Proc. 18th Int. Conf. Sorrento IAEA (Vienna, 2000)*
[20]. Kadota K. Otsuka M. and Fujita J. 1980 *Nuclear Fusion* **20** 209
[21]. Meister H. *et al* 2004 *Review of Scientific Instruments* **75** 4097
[22]. Mayoral M-L. *et al* 2009 *36th EPS Conference* ECA vol. **33E** O4-048
[23]. Mayoral M-L. *et al* 2009 *AIP Conference Proceedings of 18th Topical Conf. on RF Power in Plasmas (Gent, 2009)*

Ion	Wavelength [Å]	Transition
Ni XXVI	165.40	$1s^2\ 2s\ ^2S_{1/2} - 1s^2 2p\ ^2P_{3/2}$
Fe XXIV	192.01	$1s^2\ 2s\ ^2S_{1/2} - 1s^2 2p\ ^2P_{3/2}$
Cu XXVII	153.46	$1s^2\ 2s\ ^2S_{1/2} - 1s^2 2p\ ^2P_{3/2}$

Table 1: Li-like transitions of metallic elements used in the analyses.

	n_z	ΔZ_{eff}	Δn_{HDT}
Ni	$a = (1.73\pm1.6)\times10^{16}$	$a = (0.4\pm1.1)\times10^{19}$	$a = (3.6\pm4.5)\times10^{17}$
	$b = (3.4\pm0.5)\times10^{16}$	$b = (2.4\pm0.4)\times10^{19}$	$b = (9.0\pm1.5)\times10^{17}$
Fe	$a = (1.5\pm3.7)\times10^{16}$	$a = (0.2\pm2.2)\times10^{19}$	$a = (0.8\pm 9.4)\times10^{17}$
	$b = (3.8\pm1.4)\times10^{16}$	$b = (2.3\pm0.8)\times10^{19}$	$b = (1.0\pm0.3)\times10^{18}$
Cu	$a = (2.4\pm2.3)\times10^{16}$	$a = (0.7\pm1.8)\times10^{19}$	$a = (5.1\pm12)\times10^{17}$
	$b = (2.9\pm0.8)\times10^{16}$	$b = (2.3\pm0.6)\times10^{19}$	$b = (8.3\pm4.2)\times10^{17}$

Table 2: The linear fit coefficients of derived quantities: impurity density, ΔZ_{eff}, and dilution obtained with statistical errors for different elements, valid in the region with r/a from 0.5 to 0.6. The linear regression model is stated as y=a+bx, where the parameters a and b are derived by the method of least squares.

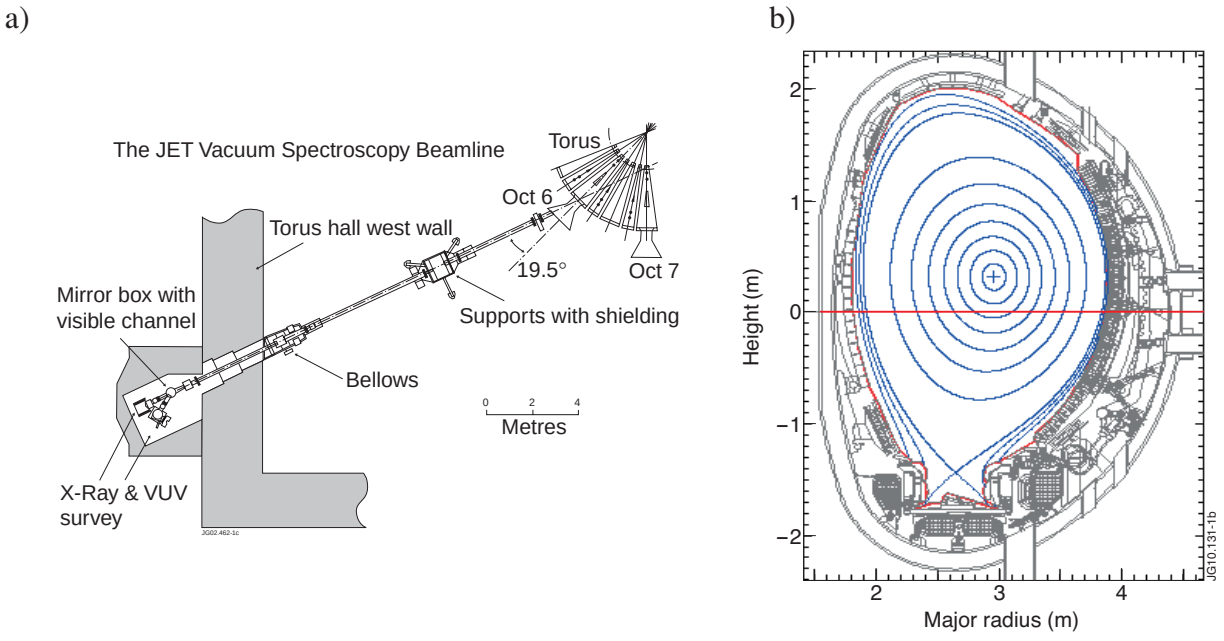

Figure 1: a) JET installation of the KT2 VUV spectrometer, b) line of sight of the diagnostic.

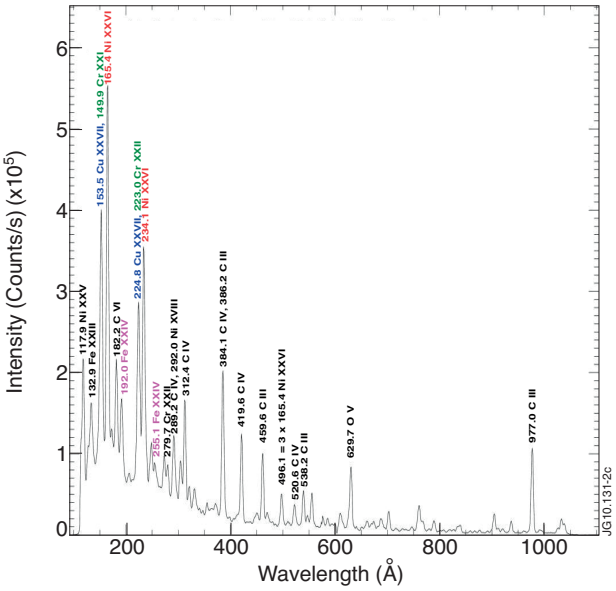

Figure 2: SPRED spectrum for JET Pulse No: 61173, averaged during 1s.

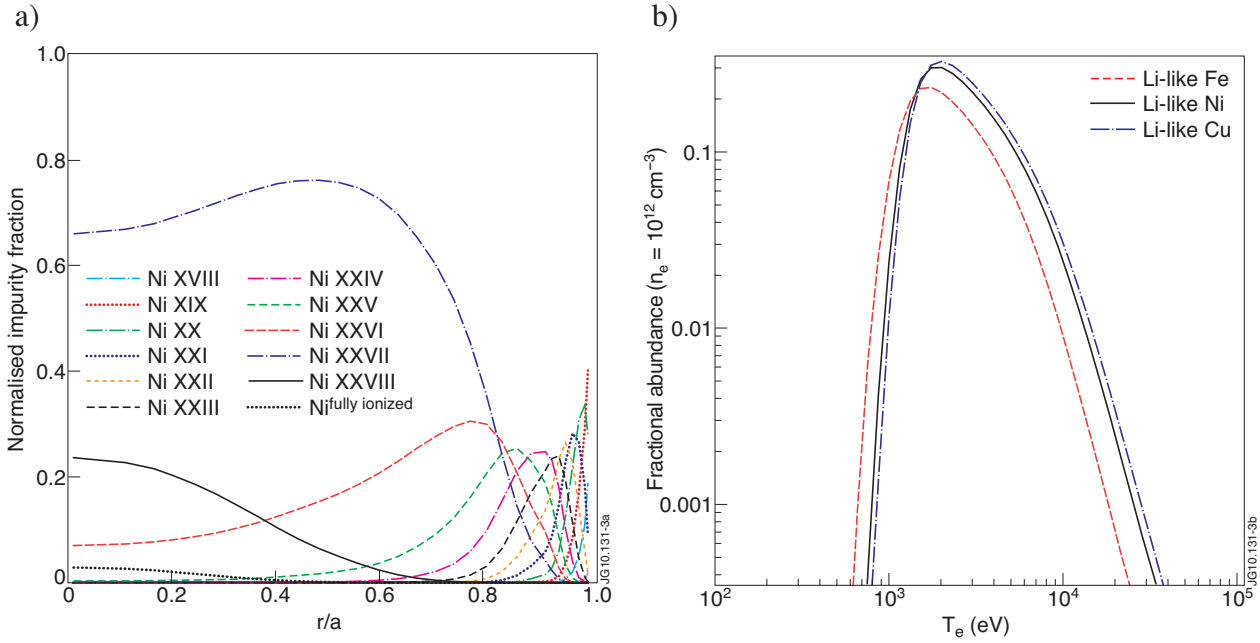

Figure 3: a) Nickel ion distribution in a JET plasma calculated for typical T_e and n_e profiles in coronal equilibrium, b) abundance of Li-like charge states for different metallic elements in coronal equilibrium.

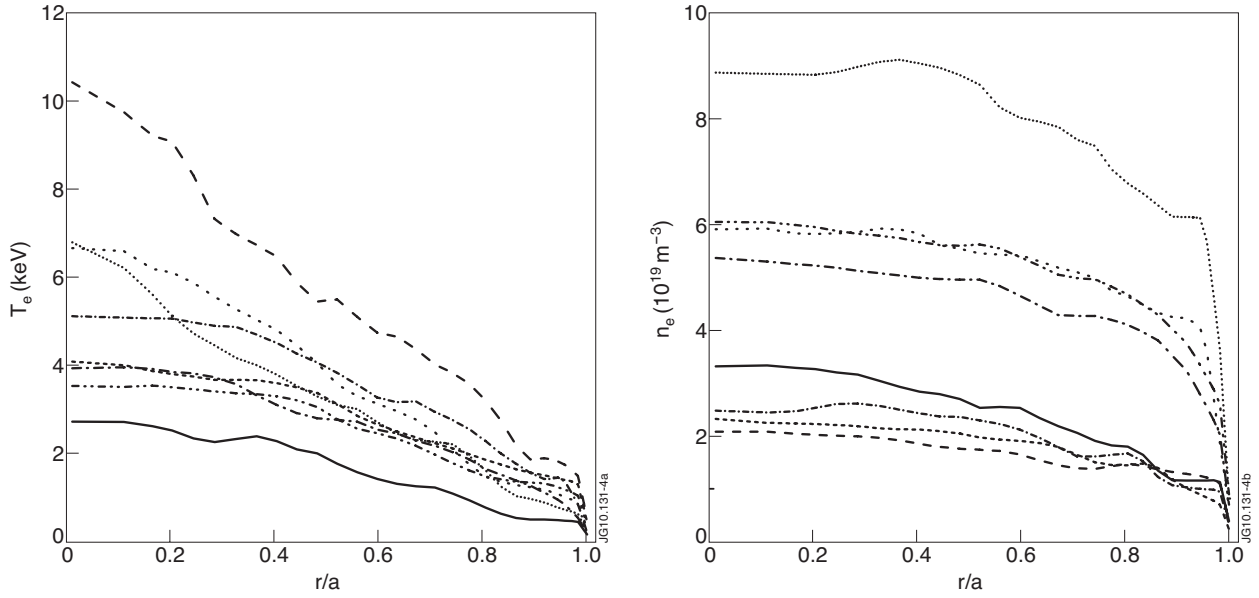

Figure 4: Electron density and temperature profiles obtained from the LIDAR Thomson scattering and electron cyclotron emission diagnostics used in UTC simulations to test different JET discharges. One T_e and one n_e profiles have been used for each Ni point in Figure 7.

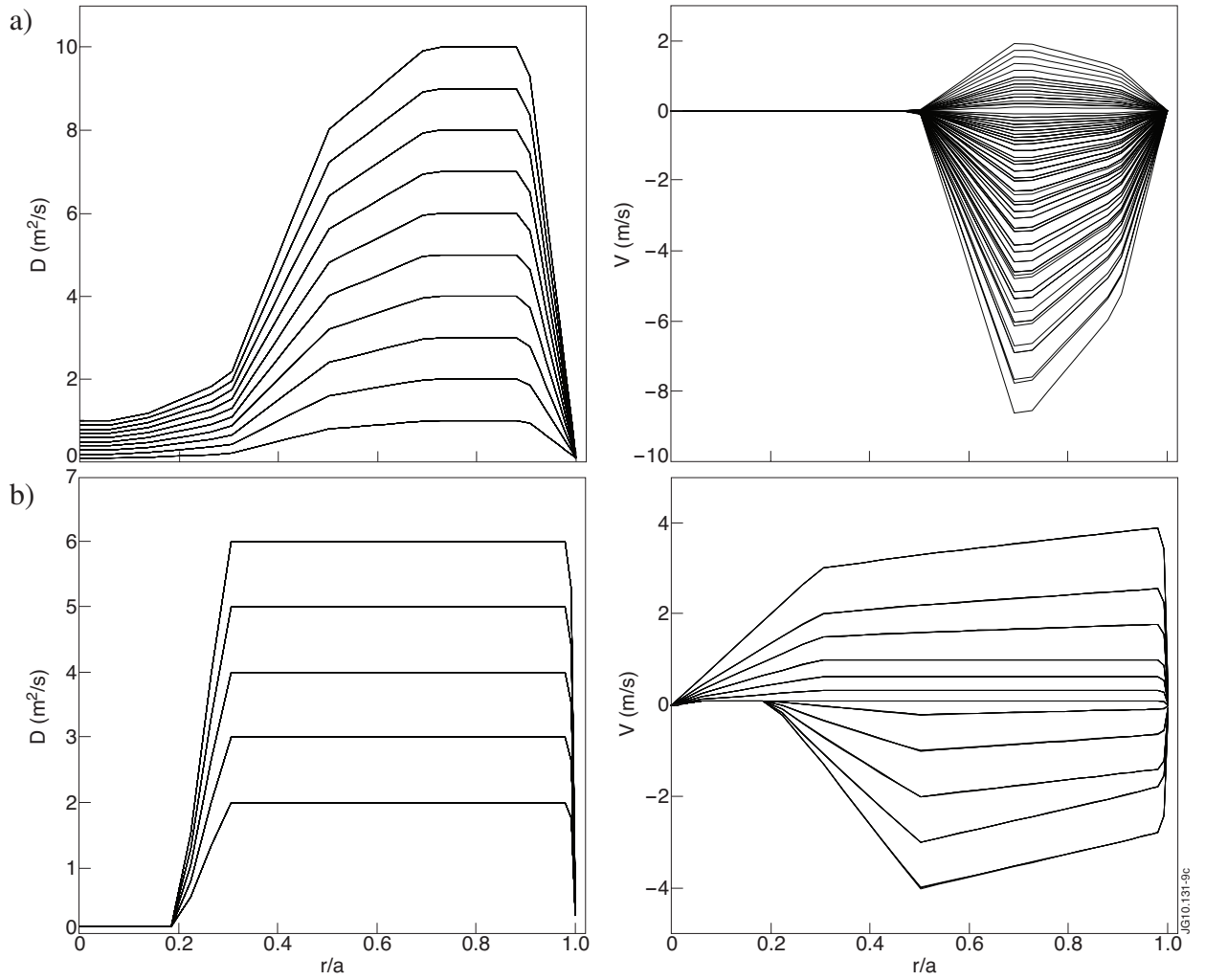

Figure 5:(a), (b) Sets of diffusion D(r) and convection v(r) transport coefficients used in UTC simulations as unknown discharge parameters in the region where the Li-like emission occurs.

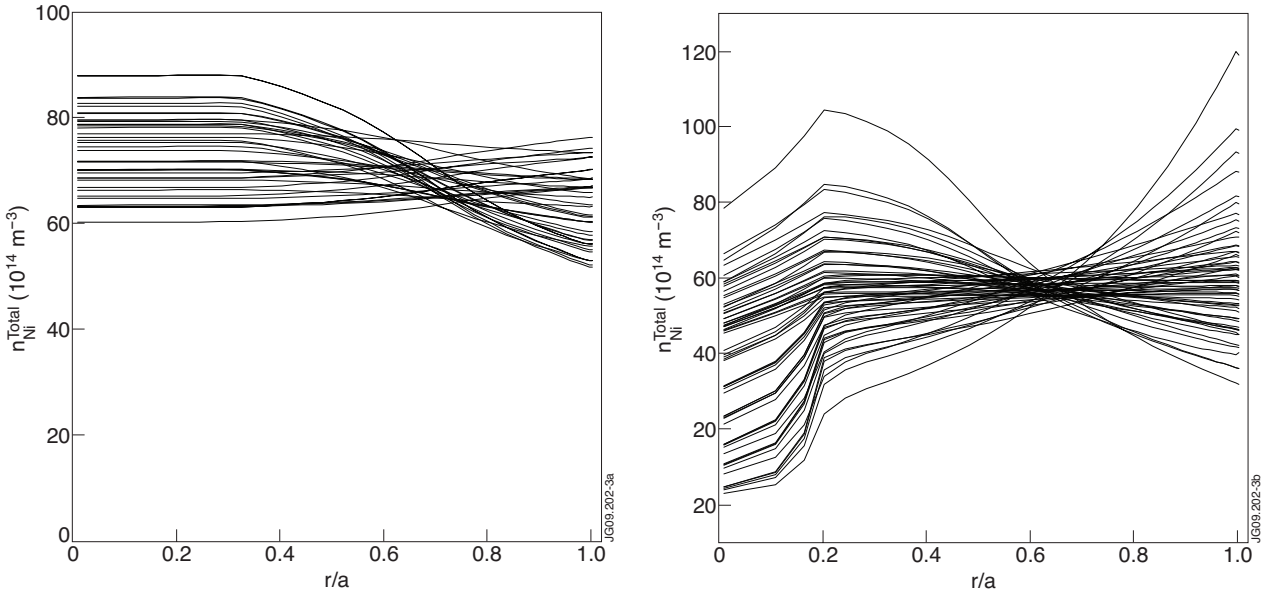

Figure 6. Total Ni density profiles obtained by means of the UTC simulations for a wide class of transport coefficients (a) presented in Figure 5(a, b) presented in Figure 5b.

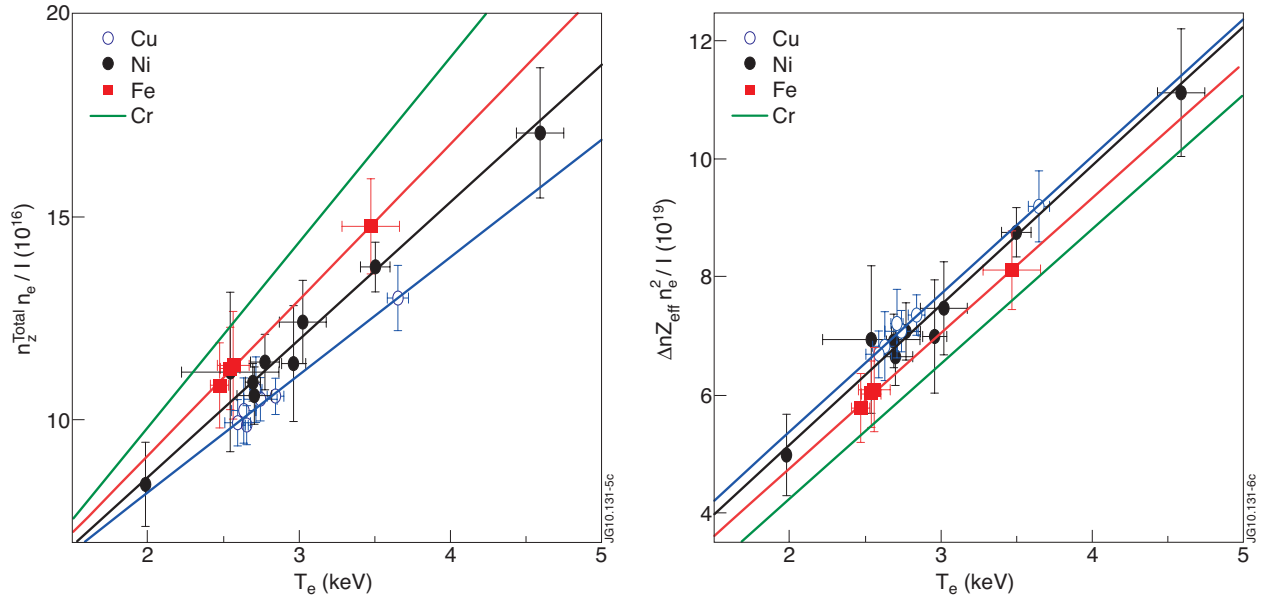

Figure 7: Ratio of the simulated impurity density to the experimental intensity of the $1s^2 2p\ ^2P_{3/2} - 1s^2 2s\ ^2S_{1/2}$ transition in Li-like Ni, Fe, Cu (normalized to the electron density) for the mid-radius region as a function of electron temperature. The green line is the extrapolated linear fit for Cr.

Figure 8: Ratio of ΔZ_{eff} to the experimental intensity of the $1s^2 2p\ ^2P_{3/2} - 1s^2 2s\ ^2S_{1/2}$ transition in Li-like Ni, Fe, Cu (normalized to the square of electron density) for the mid-radius region as a function of electron temperature. The green line is the extrapolated linear fit for Cr.

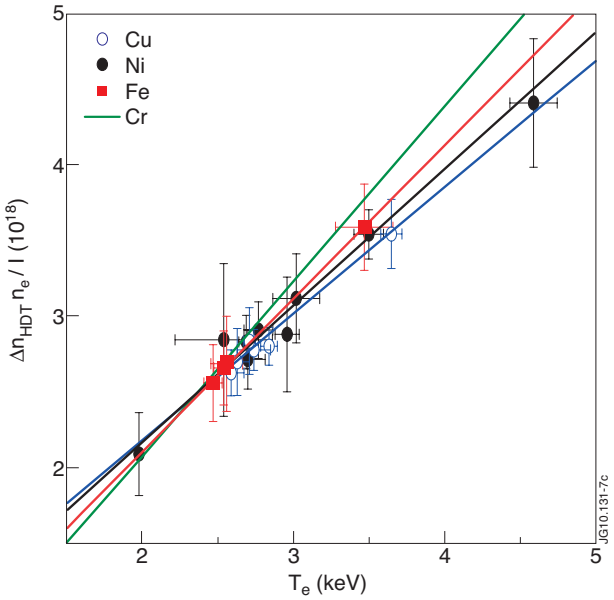

Figure 9: Ratio of dilution to the experimental intensity of the $1s^2 2p\ ^2P_{3/2} - 1s^2 2s\ ^2S_{1/2}$ transition in Li-like Ni, Fe, Cu (normalized to the electron density) for the mid-radius region as a function of electron temperature. The green line is the extrapolated linear fit for Cr.

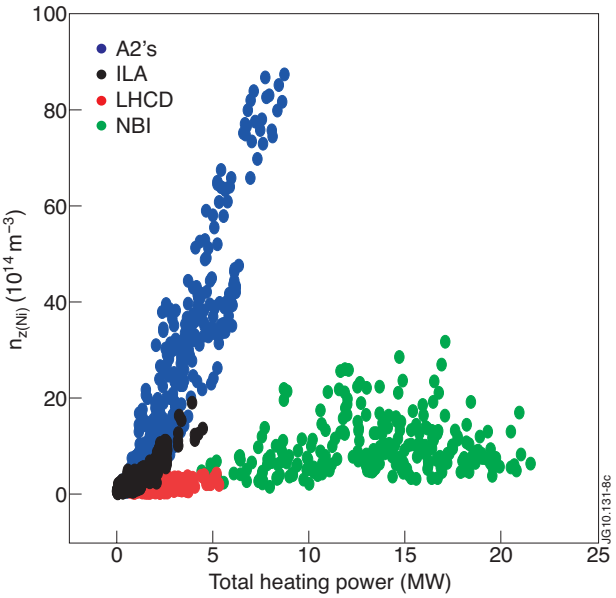

Figure 10: Correlation between the derived Ni densities (r/a~0.5–0.6) and applied heating power for different JET heating systems.